iScience

CellPress
OPEN ACCESS

Article

Mechanical overloading leads to chondrocyte degeneration and senescence via Zmpste24-mediated nuclear membrane instability

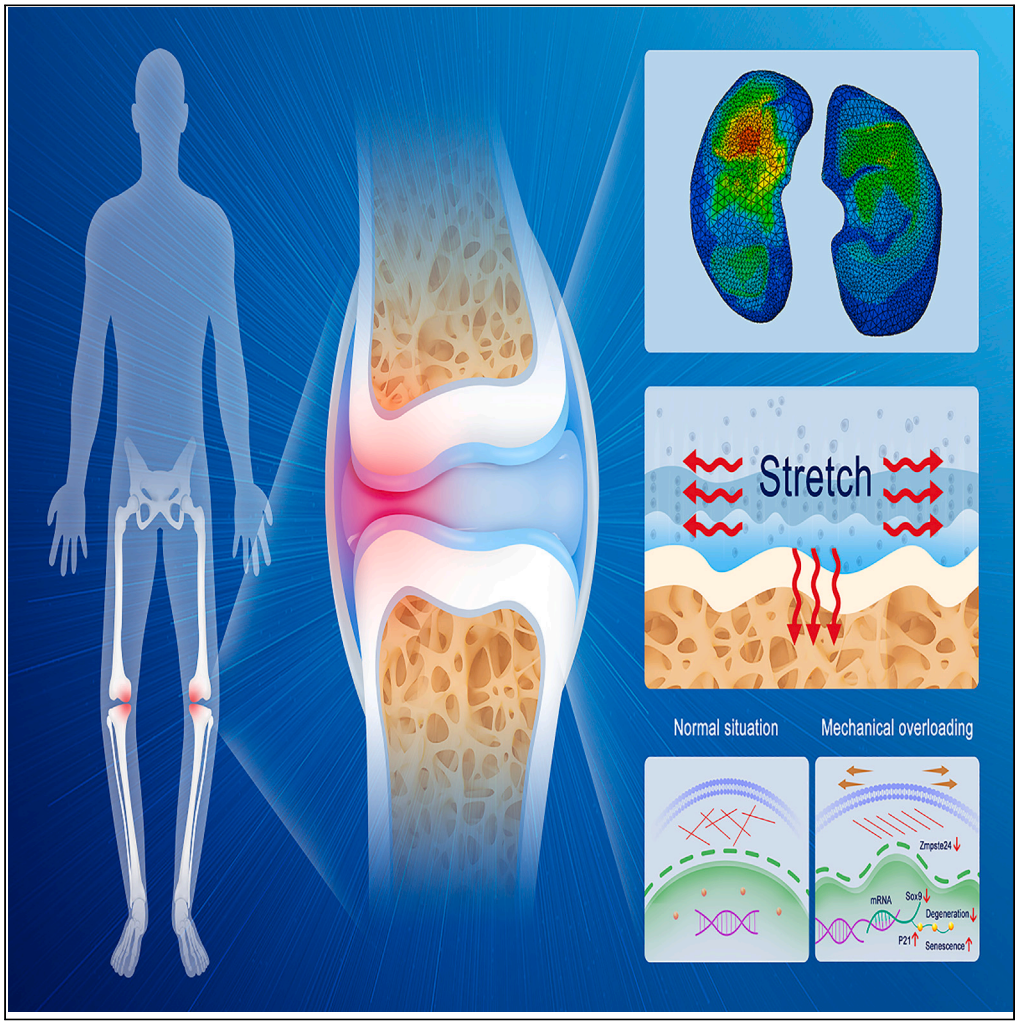

Keyu Kong, Minghao Jin, Chen Zhao, ..., Yongyun Chang, Huiwu Li, Zanjing Zhai

changyongyun@qq.com (Y.C.)
huiwu1223@163.com (H.L.)
zanjing_zhai@163.com (Z.Z.)

Highlights

Patients with varus knee experience most stress in the anteromedial tibial plateau

Zmpste24 expression decreases and nuclear instability happens under excessive stress

Zmpste24 overexpression rescues chondrocyte senescence caused by excessive stress

Kong et al., iScience 26, 108119
November 17, 2023 © 2023
https://doi.org/10.1016/j.isci.2023.108119

iScience

CellPress
OPEN ACCESS

Article

Mechanical overloading leads to chondrocyte degeneration and senescence via Zmpste24-mediated nuclear membrane instability

Keyu Kong,[1,5] Minghao Jin,[1,5] Chen Zhao,[1,5] Hua Qiao,[1] Xuzhuo Chen,[2] Baixing Li,[1] Kewei Rong,[1] Pu Zhang,[1] Yu Shan,[3] Zhengquan Xu,[4] Yongyun Chang,[1,*] Huiwu Li,[1,*] and Zanjing Zhai[1,6,*]

SUMMARY

Patients with OA and varus knees are subject to abnormal mechanical environment and objective of this study was to investigate the molecular mechanisms underlying chondrocyte senescence caused by mechanical overloading and the role of Zmpste24-mediated nuclear membrane instability in varus knees. Finite element analysis showed that anteromedial region of tibial plateau experienced the most mechanical stress in an osteoarthritis patient with a varus knee. Immunohistochemistry exhibited lower Zmpste24 expression and higher expression of senescence marker p21 in the anteromedial region. Animal experiments and cell-stretch models also demonstrated an inverse relationship between Zmpste24 and mechanically induced senescence. Zmpste24 overexpression rescued cartilage degeneration and senescence *in vitro* by scavenging ROS. In conclusion, anteromedial tibial plateau is exposed to abnormal stress in varus knees, downregulation of Zmpste24, and nuclear membrane stability may explain increased senescence in this region. Zmpste24 and nuclear membrane stability are potential targets for treating osteoarthritis caused by abnormal alignment.

INTRODUCTION

Osteoarthritis (OA) is the most common joint disease and a major cause of disability, pain, and socioeconomic burden worldwide. It is characterized by local cartilage wear, subchondral osteosclerosis, and the formation of osteophytes.[1] There are currently many promising therapies available, such as antibodies targeting IL-1β[2] and TNF-α,[3] platelet-rich plasma,[4] stem cells,[5] and fibroblast growth factor 18 (FGF18).[6] However, there is currently no treatment that can reverse end-stage cartilage degeneration. OA is a multifactorial disease in which aging and obesity are the most prominent factors,[1] which are associated with the involvement of senescence and abnormal mechanical conditions.

The knee and hip joints are the main load-bearing joints of the lower extremities and experience large compressive contact stresses during daily activities.[7] The knee joint cartilage is mainly subdivided into four zones, from the articulating surface toward the subchondral bone[8]: the superficial, intermediate (transitional layer), deep, and calcified zones. Multiple studies have shown that reasonable mechanical stimulation has a protective effect on chondrocyte metabolism by downregulating the expression of Mmp1 (Matrix metalloproteinase gene 1) and Mmp13.[9] In contrast, excessive stress results in the catabolic metabolism of chondrocytes and accelerates the degradation of the cartilage matrix.[10–12] A prospective longitudinal cohort study demonstrated that both varus and valgus alignments increase the risk of knee OA progression.[13] High tibial osteotomy (HTO) is widely used in clinical practice and have achieved satisfactory outcomes, which indicates close relation between alignment and osteoarthritis.[14] Thus, the exploration of mechanisms under mechanical overloading-induced cartilage degeneration and development of non-invasive therapy showed great significance. To date, no studies have reported the role of nuclear membrane stability in stress-induced cartilage degeneration.

In addition to obesity, cellular senescence is an important factor that leads to OA.[15–17] Senescent cells will secrete harmful pro-inflammatory molecules into the surrounding microenvironment such as IL-6, IL-1β, and Mmps, which is known as the senescence-associated secretory phenotype (SASPs).[18,19] Senescent cells have been found in the cartilage of patients with OA.[15] Jeon et al.[20] showed that the local clearance of senescent cells in cartilage alleviated the progression of OA. In the etiology of OA, senescence and mechanical overloading are often

[1]Shanghai Key Laboratory of Orthopaedic Implants, Department of Orthopaedic Surgery, Shanghai Ninth People's Hospital, Shanghai Jiaotong University School of Medicine, Shanghai, China
[2]Shanghai Key Laboratory of Stomatology, Department of Oral Surgery, College of Stomatology, Ninth People's Hospital, Shanghai Research Institute of Stomatology, National Clinical Research Center of Stomatology, Shanghai Jiao Tong University School of Medicine, Shanghai, China
[3]Suzhou Ninth People's Hospital, Department of Orthopedics, Suzhou Ninth Hospital affiliated to Soochow University, Suzhou, China
[4]Suzhou Municipal Hospital, Department of Orthopedics, Suzhou Hospital Affiliated to Nanjing Medical University, Suzhou, China
[5]These authors contributed equally
[6]Lead contact
*Correspondence: changyongyun@qq.com (Y.C.), huiwu1223@163.com (H.L.), zanjing_zhai@163.com (Z.Z.)
https://doi.org/10.1016/j.isci.2023.108119

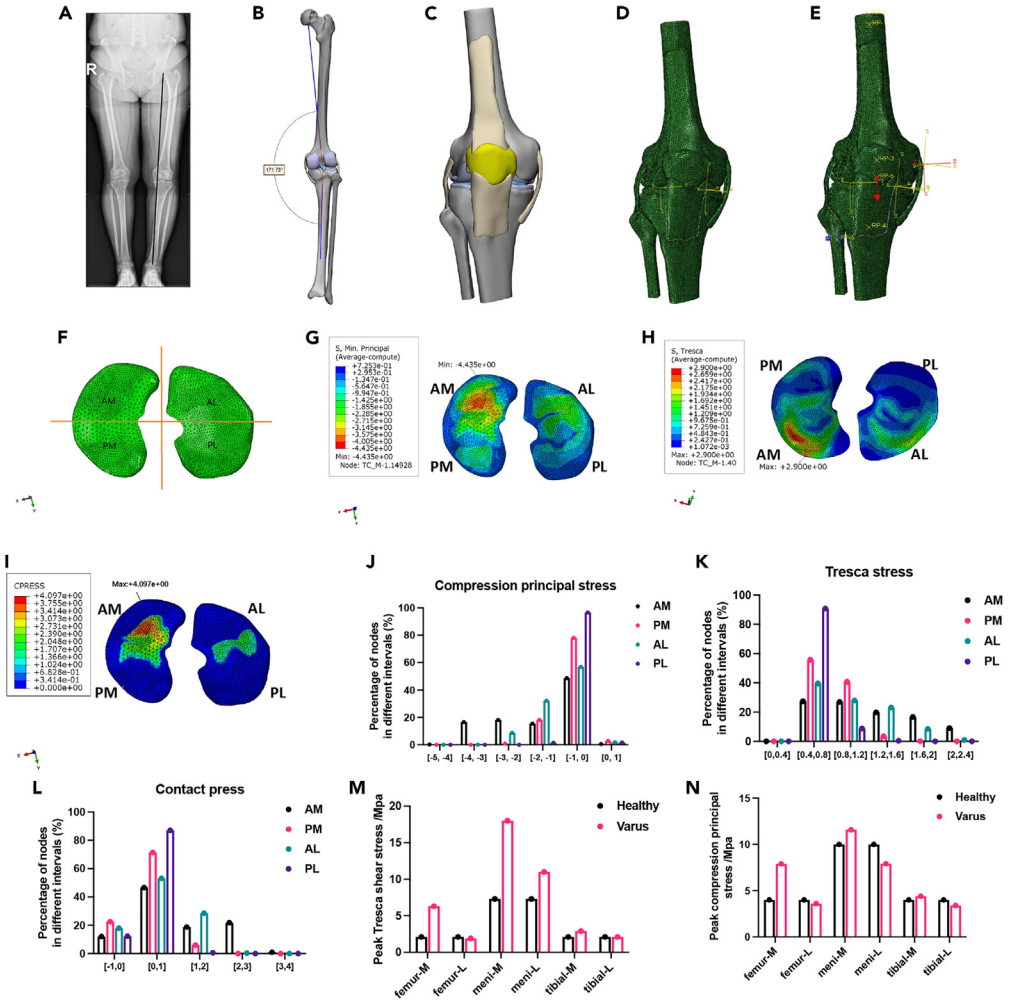

Figure 1. Modeling and finite element analysis procedures

(A) Representative X-ray of patients with OA with varus knees.

(B and C) Reconstruction of the right lower extremity of patients.

(D and E) Finite element model and loading condition for knee joint.

(F) Division of four different regions on the tibial cartilage plateau.

(G–I) Distribution of compression principal stress, Tresca stress, and contact pressure on tibial cartilage.

(J–L) Percentage of nodes in different stress intercals of compression principal stress, Tresca stress, and contact pressure in different regions.

(M and N) Comparison of peak Tresca shear stress and peak compression principal stress between healthy volunteers and patients with OA with varus knees.

regarded as independent factors. In recent years, a few studies have explored their relationship and found that oxidative stress,[21,22] ubiquitin ligase,[10] microRNA,[23] and estrogen receptors[24] all played a role in this interplay. However, the role of Zmpste24-mediated nuclear instability in mechanical overloading-related chondrocyte senescence has not been studied yet.

Zmpste24 is a zinc metalloproteinase that plays an important role in the maturation of Lamin A by cleaving the protein.[25] Lamin A is the main component of the nuclear membrane, and accumulation of its immature form, prelamin A, influences nuclear architecture and mechanics,[26] which subsequently causes genomic instability and DNA damage.[27] Zmpste24 knockout mice exhibit significant premature aging phenotypes, including spontaneous bone fractures and muscle weakness. In a recent study by Suo et al.,[28] Zmpste24 deficiency accelerated cartilage senescence and degeneration. Other studies[29] also suggested that Lamin A and nuclear stability play important roles in the mechanosensation of alveolar cells during mechanical ventilation. However, whether the reduction in Zmpste24 expression and nuclear membrane stability is involved in mechanical overloading of chondrocytes remains unknown.

A better understanding of the molecular mechanisms underlying the interplay between mechanical stress and cartilage senescence in cartilage biology will aid efforts to delay the onset and progression of OA. In our study, we constructed a finite element analysis (FEA) model of patients with OA with varus knees and mouse models with mechanical instability to investigate

Table 1. Material properties of the meniscus

Structure	Material behavior	Material constants
Meniscus	transversely anisotropic	E1 = E3 = 20Mpa, E2 = 120Mpa,V13 = 0.2, V12 = V23 = 0.3, G12 = G23 = 57.7Mpa,G13 = 8.33Mpa

the following: 1. Stress distribution on the tibial plateau cartilage in patients with OA with varus knees. 2. The relationship between stress distribution and expression of p21, a marker of senescent cells, and Zmpste24 in patients with OA and mice. 3. Whether maintaining nuclear stability by overexpressing Zmpste24 *in vitro* can rescue chondrocyte senescence and degeneration caused by excessive mechanical stress.

RESULTS

Mechanical stress is concentrated in the anteromedial (AM) area of the tibial plateau in patients with OA and varus knees.

The tibial cartilage surface was divided into four regions: anteromedial (AM), anterolateral (AL), posteromedial (PM), and posterolateral (PL; Figure 1F). Principal compression stress was used to characterize the compressive state of the cartilage. Material properties of meniscus and ligament were illustrated in Tables 1 and 2. The femoral, meniscus, and tibial cartilages experienced higher stress levels in the AM (Figures 1G; Figures S1A and S1B). The peak compressive principal stress of the femoral cartilage was 7.96 Mpa, whereas that of the meniscus was 11.6 Mpa. That of the tibial cartilage was 4.44 Mpa. As shown in Figure 1J, the compressive stress in the AM region was highest, and the percentage of nodes with a compressive stress greater than 2 MPa was more than 34%, whereas that in the AL region was 9%, that in the PM region was 0.8%, and that in the PL region was 0%. The average principal compressive stresses in the four regions were AM: −1.42 Mpa, AL: −0.88 Mpa, PM: −0.51 Mpa, PL: −0.26 Mpa, respectively.

The Tresca stress was used to characterize the shear state of the cartilage. The maximum shear force was observed on the contact surface between the cartilage and the bone, and the highest Tresca stress level was observed in the AM region (Figures 1H; Figures S1C and S1D). The shear stress on the AM area was larger, and the abundance of nodes with shear stress greater than 1.6 Mpa was more than 25.7%, whereas that of the AL area was 9.3%, the PM area was 0.1%, and the PL area was 0% (Figure 1K). The average Tresca shear stress in the four regions was, AM: 0.84 Mpa, AL: 0.61 Mpa, PM: 0.35 Mpa, PL: 0.19 Mpa.

The contact pressure represents the surface pressure caused by contact. The maximum contact pressure occurs on the contact surface between the cartilage and bone. As shown in Figures 1I and Figures S1E and S1F, the contact pressure on the AM area was largest, in which the amount of contact pressure greater than 2 MPa was more than 22.7%, while that of the AL area was 0.4%, that the PM area was 0%, and the PL area was 0% (Figure 1L). The average contact pressures in the four regions were AM:0.95 Mpa, AL: 0.57 Mpa, PM:0.31 Mpa, PL: 0.15 Mpa.

The maximum principal compressive stress and Tresca shear stress obtained from this analysis were compared with the calculated results for healthy knees[30] under the same load conditions, as shown in Figures 1M and 1N.

Zmpste24 was downregulated and p21 was upregulated in the anteromedial area of the tibial plateau, and a linear correlation existed between them

As shown in Figure 2A, we drilled a plug at the center of each of the four regions (AM, AL, PM, and PL) and performed subsequent histological and immunohistochemical staining. Demographic statistics of all included patients were collected in Table 3. The results showed that cartilage wear in the AM region was the most severe, with vertical cleft/erosion extending to 50–75% of the cartilage (Figure 2B). Most specimens showed an OARSI score of 5 (Figure 2C), and the wear state in the PM area was relatively mild, with most OARSI scores ranging from 2 to 4. In contrast, there was almost no abrasion in the AL and PL regions and most scores were 2 points or less. The most severe cartilage wear in the AM area was consistent with the maximum stress in this area. The IHC results showed that the expression of p21 in the AM region was the highest (Figures 2B and 2D), whereas there was no significant difference in the expression levels among the other three groups. The expression of Zmpste24 in the AM region was lower than that in the other three groups (Figures 2B and 2E), and there was no significant difference among the other three groups. Linear regression analysis of

Table 2. Material properties of the ligaments

Structure	Material behavior	Material constants
colateral ligament (LCL)	Neo-Hookean: $\Psi = C1(\bar{I}_1 - 3)$	C1 = 6.06
medial colateral ligament (MCL)		C1 = 6.43
anterior cruciate ligament (ACL)		C1 = 5.83
posterior cruciate ligament (PCL)		C1 = 6.06
patellar tendon (PT)		C1 = 2.75

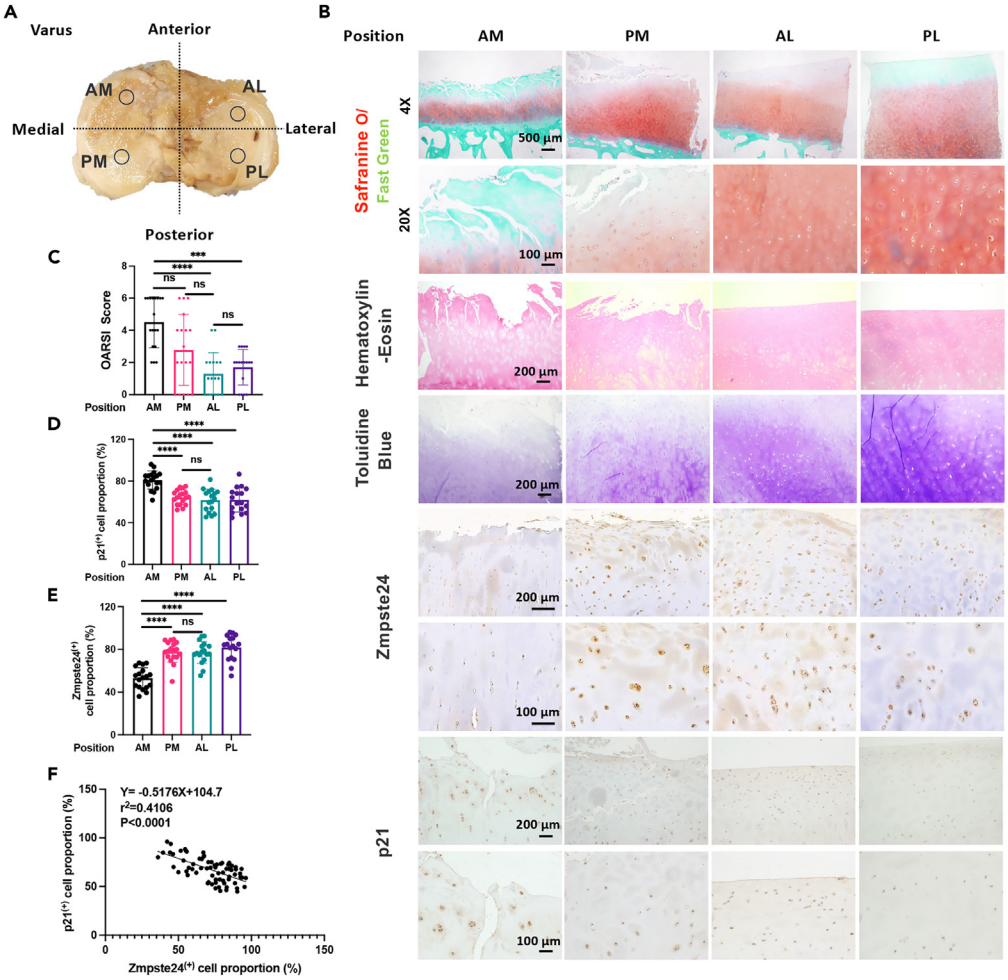

Figure 2. Expression of p21 and Zmpste24 in different regions of tibial cartilage from patients with varus undergoing TKA and the relationship between them

(A) Schematic plot of plug drilling in different regions of the tibial plateau from patients with varus undergoing TKA.

(B) Representative images of Safranine O/Fast green, H&E, Toluidine blue, and IHC staining of p21 and Zmpste24 in different regions.

(C–E) Analysis of OARSI scores, p21 positive cells, and Zmpste24 positive cells of specimens in different regions.

(F) Pearson correlation analysis and simple linear regression between the expression of p21 and Zmpste24. *$p < 0.05$, **$p < 0.01$, ***$p < 0.001$, and ****$p < 0.0001$.

the expression levels of Zmpste24 and p21 showed a negative correlation between them, with an r^2 of 0.4106, and the regression equation was Y = −0.5176X+104.7 (Figure 2F). In summary, the magnitude of cartilage stress is directly proportional to the expression of p21 and inversely proportional to the expression of Zmpste24. Excessive stress on cartilage leads to chondrocyte senescence, therefore Zmpste24 may be involved in this process.

Zmpste24 expression was downregulated and p21 expression was upregulated in the medial plateau cartilage of destabilization of the medial meniscus-treated mice

As it is difficult to obtain the tibial plateau cartilage of normal individuals and compare it with the cartilage of patients with varus knees, we built a mouse model of medial meniscus instability and changed the alignment of their lower limbs. Previous studies[31] have reported that the DMM model can increase stress on the medial tibial cartilage. Thus, we reconstructed and analyzed the subchondral bone of mice in the Sham and DMM groups and found that the subchondral bone of mice in the DMM group was significantly reconstructed, with substantial subchondral bone sclerosis, which may further exacerbate abnormal cartilage mechanical conduction (Figures 3A and 3B). HE and Safranine O/Fast green staining illustrated that most abrasion occurred in the medial cartilage (Figures 3C and 3D). IF staining analysis showed that the expressions of Col2a1 and Zmpste24 decreased and that of p21 increased in the medial tibial cartilage of DMM group mice, which was consistent with the results in patient specimens (Figures 3E and 3F). In addition, linear regression analysis of the

Table 3. Demographic statistics of patients whose cartilage samples were used in this study

I.D.	Age	Sex	Kellgren-Lawrence (KL) grade
1	56	F	3
2	72	M	3
3	74	M	4
4	76	M	4
5	74	F	2
6	65	F	4
7	68	F	2
8	76	F	4
9	77	F	4
10	59	F	4
11	85	M	2
12	80	F	3
13	76	F	2
14	59	F	3
15	58	M	2
16	79	F	4
17	75	F	3
18	71	F	4

expression levels of Zmpste24 and p21 in cartilage showed a negative correlation between them, with an r^2 of 0.6178, and the regression equation was Y = −0.7613X+76.15 (Figure 3G)

Zmpste24 downregulation and nuclear instability are observed in the cell stretch model

Both human and mouse knee cartilage is located in complex environments. Therefore, we performed the tensile stimulation of chondrocytes using 5% elongation to simulate stress under physiological conditions and 20% elongation to simulate mechanical overloading under pathological conditions. The results showed that under 5% tensile force, the expression levels of Sox9 and col2a1 increased, while the expression of senescence-related genes, such as p21, p16 ^{INK4a}, and p53, matrix decomposition-related genes, such as Mmp13, and hypertrophic, fibrous marker Col10a1 and Col1a1 decreased after 12 or 24 h of stretching (Figure 4A and S2A and S2B). Simultaneously, there was no significant change in the expression of Zmpste24 (Figures 4C and 4F). Under 20% tensile force, the expression levels of Sox9 and Col2a1 decreased after different loading times, whereas those of p21, p16^{INK4a}, p53, Mmp13, Col10a1, and Col1a1 increased (Figure 4B and S2A and S2B). The number of β-gal positive cells increased, while the expression of Zmpste24 decreased under 20% tensile force (Figures 4C, 4E, and 4F). Thus, 20% tension has a negative impact on chondrocytes and Zmpste24 may be involved in this process. At the same time, we found that under 20% tension force, the cytoskeleton rearranged and the proportion of nuclear blebbing greatly increased (Figures 4C and 4D), suggesting that the nuclear membrane was unstable under mechanical overloading.

Zmpste24 overexpression rescued mechanical overloading-induced nuclear instability, chondrocyte degeneration, and senescence

In this study, we constructed a cell line that stably overexpressed Zmpste24 and subjected it to 20% tensile stress. The qRT-PCR and IF results showed successful overexpression (Figures 5A and 5E). After the overexpression of Zmpste24, mechanical overloading-induced cartilage degeneration, and senescence were significantly rescued, as shown by qRT-PCR and western blotting (Figures 5B–5D). IF staining of the nuclear membrane also showed that overexpression of Zmpste24 resulted in a more stable nuclear membrane and greater tolerance to excessive mechanical loading, as fewer cells showed nuclear blebbing after mechanical overloading (Figures 5E–5G). Furthermore, ROS generated by excessive mechanical stress was scavenged by Zmpste24 overexpression (Figures 5E and 5H).

A diagram of the role of Zmpste24 and nuclear membrane stability in cartilage degeneration and senescence under abnormal mechanical conditions was illustrated in Figure 6.

DISCUSSION

Mechanical overloading and senescence have been viewed as significant factors in osteoarthritis etiology. Based on our results, we have proved that abnormal mechanical stress was concentrated in the anteromedial regions of the tibial plateau in patients with varus. Zmpste24 downregulation plays an important role in chondrocyte senescence caused by mechanical overloading. In addition, *in vitro* experiments have

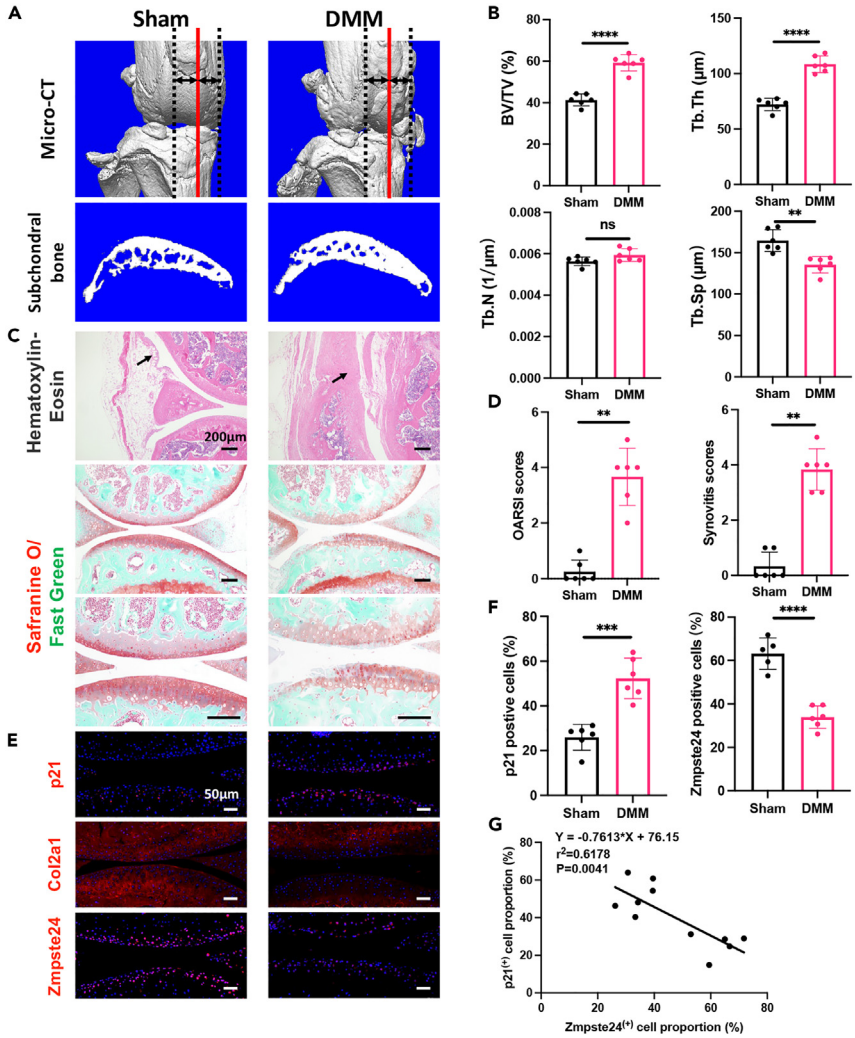

Figure 3. Zmpste24 expression is downregulated in tibial cartilage in mice with DMM surgery

(A) 3D reconstruction of the knee joints of Sham and DMM mice and representative section images of subchondral bone.

(B) Analysis of trabecular bone parameters. BV/TV, percent bone volume; Tb.N, trabecular number; Tb.Th, trabecular thickness; Tb.Sp, trabecular separation.

(C and D) H&E staining, Safranine O/Fast green, and corresponding quantitative analysis. Scale bar: 200 μm.

(E and F) IF staining of p21, Col2a1, and Zmpste24 and positive cell proportions after treatment with DMM.

(G) Pearson correlation analysis and simple linear regression between the expression of p21 and Zmpste24. Scale bar: 50 μm n = 6 in each group. *p < 0.05, **p < 0.01, ***p < 0.001, and ****p < 0.0001, compared to Sham group. Black arrow: synovium.

preliminarily proved the potential therapeutical effect of Zmpste24 overexpression in preventing mechanical overloading-induced osteoarthritis at the early stage while further *in vivo* experiments ought to be carried out in the near future.

FEA is a widely used mechanical analysis method that constructs 3D models of various structures using imaging data and mechanical parameters, such as the elastic modulus of various tissue components, which are further used to calculate the mechanical stress experienced by various tissue structures under different pathological conditions and surgical interventions.[31,32] The medial tibial cartilage and meniscus of patients with OA with varus knees who require replacement surgery are often severely worn, making it difficult to segment and reconstruct various tissues. To clarify the distribution of stress in various zones of the tibial plateau in patients with varus knees and its relationship with the expression of Zmpste24 and the aging marker p21 in the cartilage, experienced surgeons collaborated with engineers to segment soft tissues, such as ligaments and meniscus of the knee joint. A 3D model of the knee joint before surgery was successfully reconstructed, and subsequent analysis was conducted.

In our study, the tibial plateau of patients was divided into four different regions and through FEA and IHC, it was found that changes in shear force, compressive stress, and contact stress on the anteromedial zone were the most prominent and consistent with the decrease in Zmpste24 expression and increase in p21 expression. A correlation between Zmpste24 and tibial plateau cartilage stress distribution and senescence was observed in patient cartilage specimens.

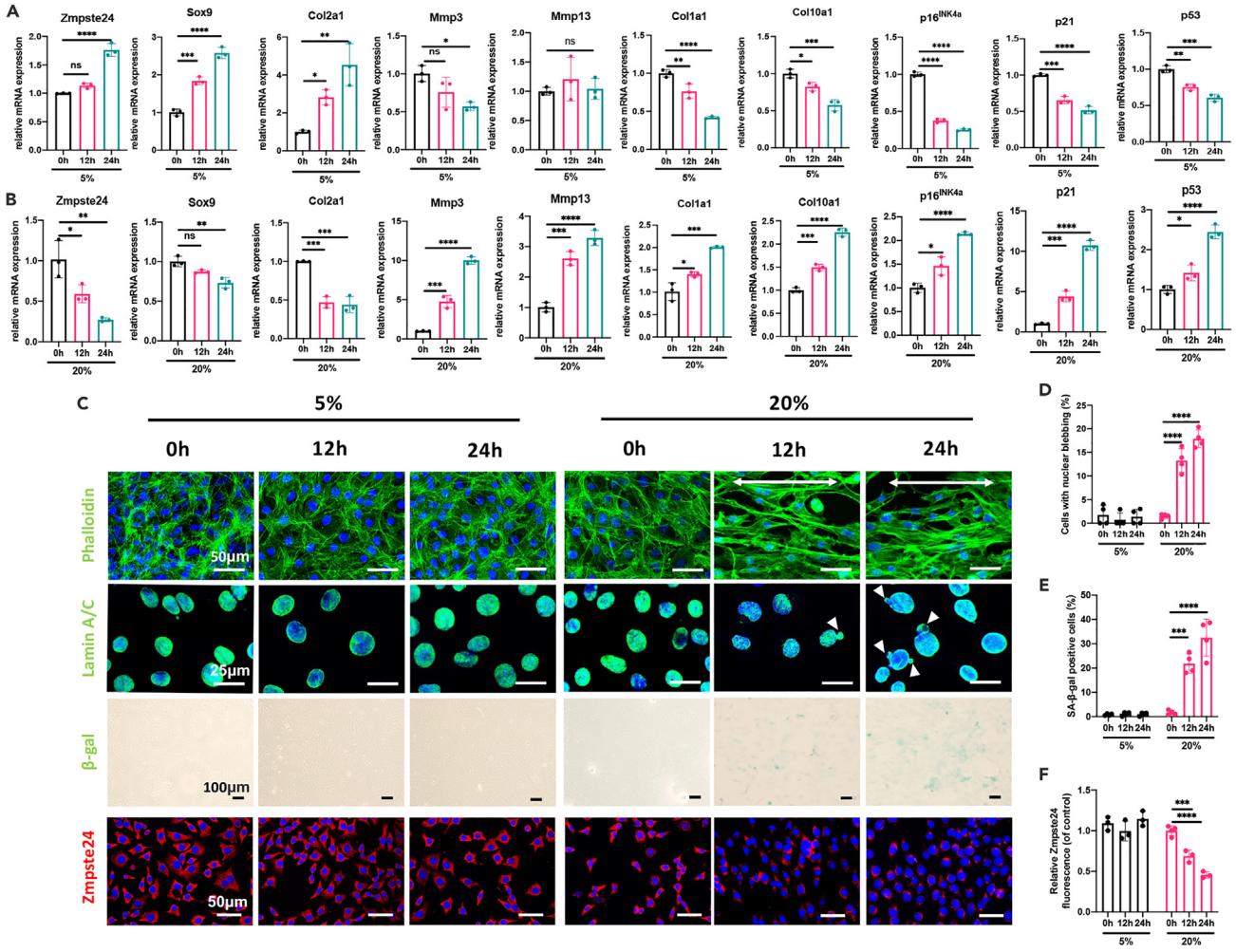

Figure 4. Excess cyclic tensile stretching induces Zmpste24 downregulated expression, nuclear membrane instability, and cell senescence in chondrocytes

(A and B) mRNA expression of Zmpte24, p21, p16^{INK4a}, p53, Col2a1, Sox9, Mmp3, Mmp13, Col1a1, and Col10a1of chondrocytes experiencing 5% or 20% elongation of cyclic tensile stretch (C–F) Presentative images of cytoskeleton, IF staining of the nuclear membrane, SA-β-gal staining of chondrocytes after different periods of 5% or 20% CTS and corresponding quantitative analysis of nuclear blebbing cell proportions, SA-β-gal positive cell proportion, and Zmpste24 fluorescence. *$p < 0.05$, **$p < 0.01$, ***$p < 0.001$, and ****$p < 0.0001$.

Nuclear membrane blebbing is a characteristic feature of cellular senescence and instability of the nuclear membrane.[33] Destabilization of the nuclear membrane further leads to changes in heterochromatin distribution, the epigenetic state of histones, and susceptibility to DNA damage.[28,34–36] Mu et al.[33] confirmed that Zmpste24 can regulate the rigidity and stiffness of the nuclear membrane and senescence of stem cells, together with the cytoskeleton. Our results also proved that under a mechanical overload environment, the chondrocyte F-actin is mostly rearranged perpendicular to the stress direction. Moreover, nuclear blebbing was evident under 20% tensile stress, whereas overexpression of Zmpste24 significantly improved the stability of the nuclear membrane and strengthened the resistance of chondrocytes to an abnormal mechanical environment. Alonso et al.[29] found that inhibiting the function of Zmpste24 and reducing nuclear stiffness made alveolar cells more resistant to the high pressure caused by mechanical ventilation. This is contradictory to our results, which show that the most suitable nuclear membrane stiffness required for different pressure types and functional organs varies, and it is necessary to strengthen or soften nuclear membranes in different mechanical environments to avoid the negative effects of excessive loading on cells. A large number of studies have explored the mechanism of cellular senescence caused by the decreased expression of Zmpste24, such as epigenetic regulation,[28] oxidative stress,[37] pytoprotection[38] and inflammation.[39] In our study, we found that mechanical overloading and subsequent downregulation of Zmpste24 will generate excess ROS and overexpression of Zmpste24 effectively scavenges it, which implicates that anti-oxidative stress may be a potential mechanism under Zmpste24 protection.

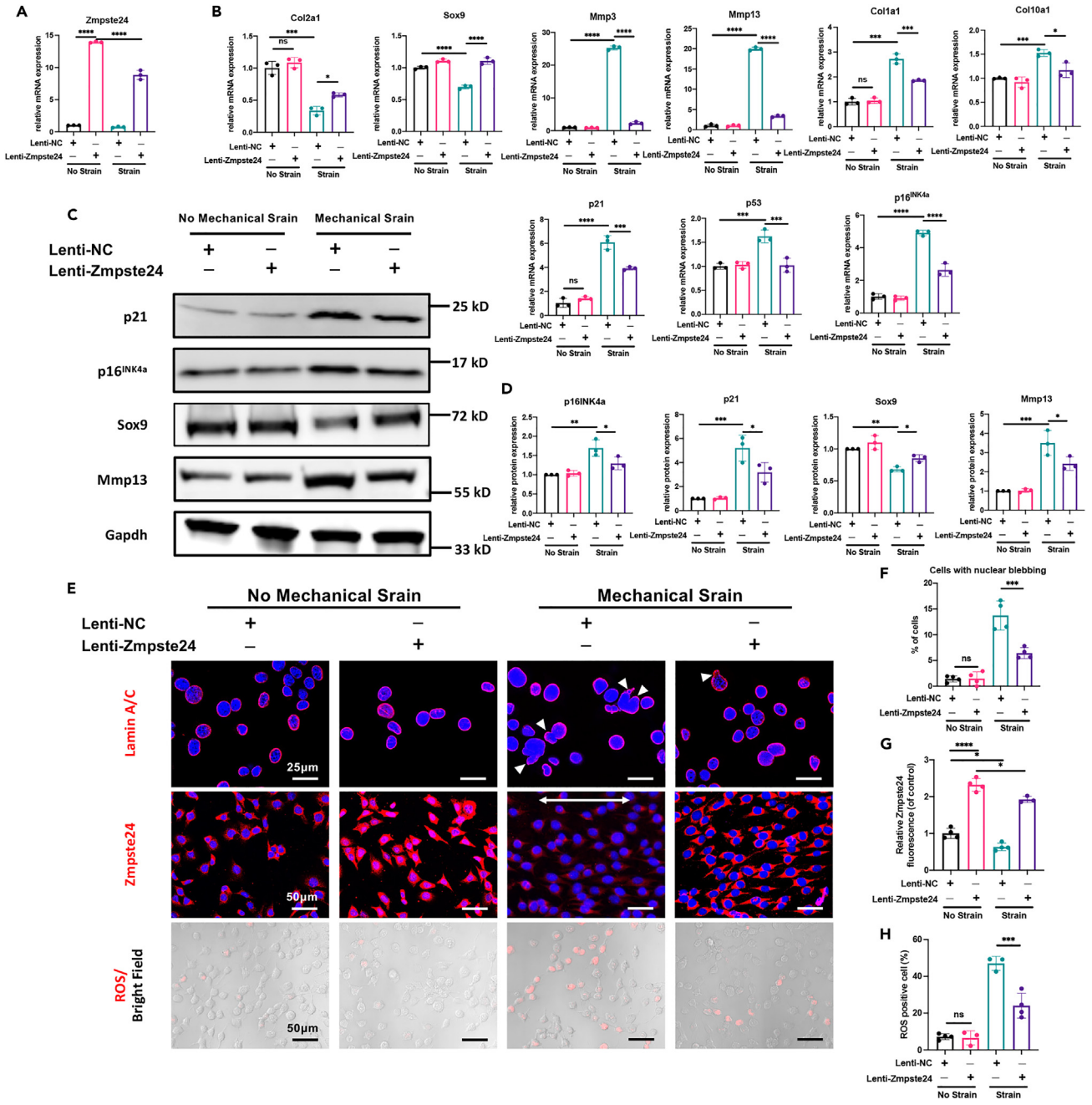

Figure 5. Overexpression of Zmpste24 could rescue mechanical overloading-induced chondrocyte degeneration and senescence *in vitro*

(A–D) Validation of Zmpste24 overexpression through qRT-PCR (B) Rescue effect of Zmpste24 overexpression on mRNA expression of Col2a1, Sox9, Mmp3, Mmp13, Col1a1, Col10a1, p16^{INK4a}, p21, and p53 (C and D) Rescue effect of Zmpste24 overexpression on protein expression of Col2a1, Sox9, Mmp3, Mmp13, p16^{INK4a}, p21, and p53 and corresponding analysis.

(E–H) IF staining of Lamin A/C, Zmpste24 and ROS and corresponding cell proportion analysis. *p < 0.05, **p < 0.01, ***p < 0.001, and ****p < 0.0001.

In conclusion, our study found, for the first time, that nuclear membrane instability caused by decreased expression of Zmpste24 may be involved in the process of chondrocyte senescence caused by different mechanic conditions, by combining FEA with IHC analysis of patients' tibial cartilage. Furthermore, we explored the protective role of Zmpste24 overexpression and nuclear stabilization in mechanic-related senescence *in vitro*. In the future, we will explore other methods besides gene editing therapy to stabilize the nuclear membrane, thereby providing more treatment options for mechanical abnormality-related diseases.

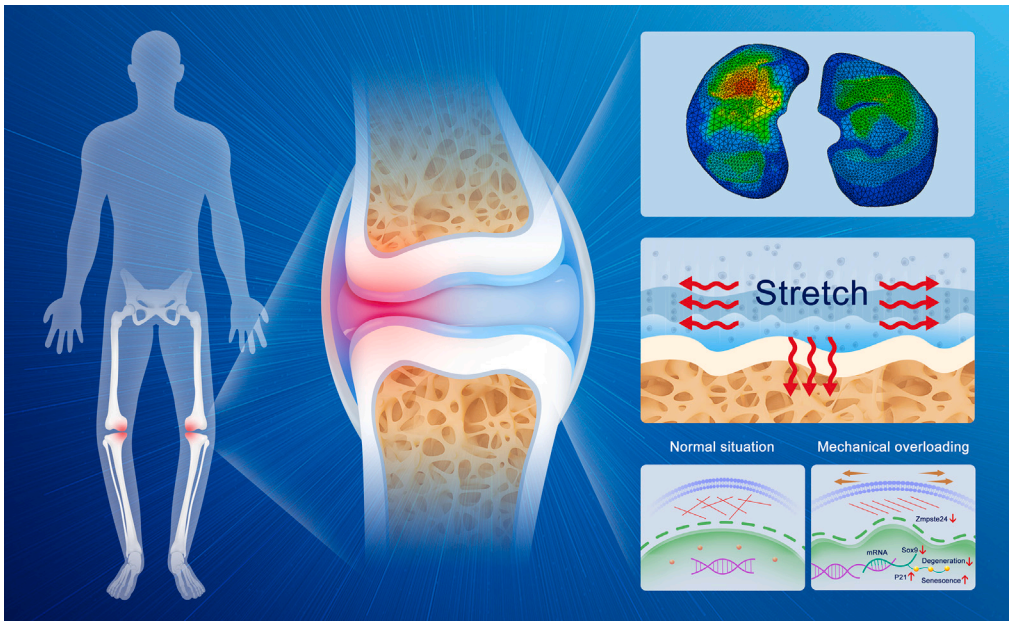

Figure 6. The role of Zmpste24 and nuclear membrane stability in cartilage degeneration and senescence under abnormal mechanical conditions

Limitations of the study

This study has certain limitations. First, we only explored the relationship between Zmpste24 and mechanically induced aging in patients with varus and medial meniscal destabilization. Consequently, similar research should be conducted on cartilage specimens from patients with OA with valgus alignment. Second, we only observed the protective effect of Zmpste24 overexpression *in vitro*. In a subsequent study, we will inject Zmpste24 overexpressing adeno-associated virus (AAV) into mouse knee joints to further verify the effectiveness of Zmpste24 overexpression. Finally, we only concentrated on the expression of p21 and Zmpste24 in the tibial plateau, instead of in the femoral cartilage and meniscus because of the difficulty in obtaining complete femoral cartilage from TKA surgery.

STAR★METHODS

Detailed methods are provided in the online version of this paper and include the following:

- KEY RESOURCES TABLE
- RESOURCE AVAILABILITY
  - Lead contact
  - Materials availability
  - Data and code availability
- EXPERIMENTAL MODEL AND STUDY PARTICIPANT DETAILS
  - Human cartilage specimen collection and preparation
  - Animals and surgical procedures
  - Cell culture and reagents
  - Overexpression of Zmpste24 in ATDC5 cells
- METHODS DETAILS
  - Imaging data acquisition and geometric modeling
  - FEA and material models
  - Loads, boundary conditions, and contact interrelationships
  - Micro-CT scanning
  - Histology, immunohistochemistry (IHC), and immunofluorescence (IF) staining
  - Cyclic tensile strain loading of chondrocytes
  - Senescence-associated-β-galactosidase (SA-β-gal) staining
  - Detection of reactive oxygen species (ROS)
  - Protein extraction and western blot analysis
- QUANTIFICATION AND STATISTICAL ANALYSIS
  - Statistical analysis

SUPPLEMENTAL INFORMATION

Supplemental information can be found online at https://doi.org/10.1016/j.isci.2023.108119.

ACKNOWLEDGMENTS

This study was supported by the National Natural Science Foundation of China (81672181, 81601958, 82072397), The Youth Talent Program from Shanghai Health System (2022YQ020), Fundamental Research Funds for the Central Universities (YG2023ZD15), and the Natural Science Foundation of Shanghai (23ZR1437300).

AUTHOR CONTRIBUTIONS

KK, MJ, and CZ performed most of the *in vitro* and *in vivo* experiments and drafted the article. HQ, XC, KR, PZ, and BL analyzed the data and participated in most of the *in vivo* experiments. YC, ZZ, and HL designed the study and revised the article. All the authors have read and approved the article.

DECLARATION OF INTERESTS

The authors declare that they have no competing interests.

INCLUSION AND DIVERSITY

We support inclusive, diverse, and equitable conduct of research.

Received: July 22, 2023
Revised: August 28, 2023
Accepted: September 29, 2023
Published: October 4, 2023

REFERENCES

1. Glyn-Jones, S., Palmer, A.J.R., Agricola, R., Price, A.J., Vincent, T.L., Weinans, H., and Carr, A.J. (2015). Osteoarthritis. Lancet *386*, 376–387. https://doi.org/10.1016/s0140-6736(14)60802-3.
2. Chevalier, X., Goupille, P., Beaulieu, A.D., Burch, F.X., Bensen, W.G., Conrozier, T., Loeuille, D., Kivitz, A.J., Silver, D., and Appleton, B.E. (2009). Intraarticular injection of anakinra in osteoarthritis of the knee: a multicenter, randomized, double-blind, placebo-controlled study. Arthritis Rheum. *61*, 344–352. https://doi.org/10.1002/art.24096.
3. Wang, J. (2018). Efficacy and safety of adalimumab by intra-articular injection for moderate to severe knee osteoarthritis: An open-label randomized controlled trial. J. Int. Med. Res. *46*, 326–334. https://doi.org/10.1177/0300060517723182.
4. Dório, M., Pereira, R.M.R., Luz, A.G.B., Deveza, L.A., de Oliveira, R.M., and Fuller, R. (2021). Efficacy of platelet-rich plasma and plasma for symptomatic treatment of knee osteoarthritis: a double-blinded placebo-controlled randomized clinical trial. BMC Musculoskelet. Disord. *22*, 822. https://doi.org/10.1186/s12891-021-04706-7.
5. Trounson, A., and McDonald, C. (2015). Stem Cell Therapies in Clinical Trials: Progress and Challenges. Cell Stem Cell *17*, 11–22. https://doi.org/10.1016/j.stem.2015.06.007.
6. Hochberg, M.C., Guermazi, A., Guehring, H., Aydemir, A., Wax, S., Fleuranceau-Morel, P., Reinstrup Bihlet, A., Byrjalsen, I., Ragnar Andersen, J., and Eckstein, F. (2019). Effect of Intra-Articular Sprifermin vs Placebo on Femorotibial Joint Cartilage Thickness in Patients With Osteoarthritis: The FORWARD Randomized Clinical Trial. JAMA *322*, 1360–1370. https://doi.org/10.1001/jama.2019.14735.
7. Carter, D.R., Beaupré, G.S., Wong, M., Smith, R.L., Andriacchi, T.P., and Schurman, D.J. (2004). The mechanobiology of articular cartilage development and degeneration. Clin. Orthop. Relat. Res. *427* (*Suppl*), S69–S77. https://doi.org/10.1097/01.blo.0000144970.05107.7e.
8. Carballo, C.B., Nakagawa, Y., Sekiya, I., and Rodeo, S.A. (2017). Basic Science of Articular Cartilage. Clin. Sports Med. *36*, 413–425. https://doi.org/10.1016/j.csm.2017.02.001.
9. He, Z., Leong, D.J., Zhuo, Z., Majeska, R.J., Cardoso, L., Spray, D.C., Goldring, M.B., Cobelli, N.J., and Sun, H.B. (2016). Strain-induced mechanotransduction through primary cilia, extracellular ATP, purinergic calcium signaling, and ERK1/2 transactivates CITED2 and downregulates MMP-1 and MMP-13 gene expression in chondrocytes. Osteoarthritis Cartilage *24*, 892–901. https://doi.org/10.1016/j.joca.2015.11.015.
10. Zhang, H., Shao, Y., Yao, Z., Liu, L., Zhang, H., Yin, J., Xie, H., Li, K., Lai, P., Zeng, H., et al. (2022). Mechanical overloading promotes chondrocyte senescence and osteoarthritis development through downregulating FBXW7. Ann. Rheum. Dis. *81*, 676–686. https://doi.org/10.1136/annrheumdis-2021-221513.
11. Bleuel, J., Zaucke, F., Brüggemann, G.P., and Niehoff, A. (2015). Effects of cyclic tensile strain on chondrocyte metabolism: a systematic review. PLoS One *10*, e0119816. https://doi.org/10.1371/journal.pone.0119816.
12. Zhang, C., Lin, S., Li, T., Jiang, Y., Huang, Z., Wen, J., Cheng, W., and Li, H. (2017). Mechanical force-mediated pathological cartilage thinning is regulated by necroptosis and apoptosis. Osteoarthritis Cartilage *25*, 1324–1334. https://doi.org/10.1016/j.joca.2017.03.018.
13. Sharma, L., Song, J., Felson, D.T., Cahue, S., Shamiyeh, E., and Dunlop, D.D. (2001). The role of knee alignment in disease progression and functional decline in knee osteoarthritis. JAMA *286*, 188–195. https://doi.org/10.1001/jama.286.2.188.
14. Murray, R., Winkler, P.W., Shaikh, H.S., and Musahl, V. (2021). High Tibial Osteotomy for Varus Deformity of the Knee. J. Am. Acad. Orthop. Surg. Glob. Res. Rev. *5*, e21.00141. https://doi.org/10.5435/JAAOSGlobal-D-21-00141.
15. Price, J.S., Waters, J.G., Darrah, C., Pennington, C., Edwards, D.R., Donell, S.T., and Clark, I.M. (2002). The role of chondrocyte senescence in osteoarthritis. Aging Cell *1*, 57–65. https://doi.org/10.1046/j.1474-9728.2002.00008.x.
16. Coryell, P.R., Diekman, B.O., and Loeser, R.F. (2021). Mechanisms and therapeutic implications of cellular senescence in osteoarthritis. Nat. Rev. Rheumatol. *17*, 47–57. https://doi.org/10.1038/s41584-020-00533-7.
17. Toh, W.S., Brittberg, M., Farr, J., Foldager, C.B., Gomoll, A.H., Hui, J.H.P., Richardson, J.B., Roberts, S., and Spector, M. (2016). Cellular senescence in aging and osteoarthritis. Acta Orthop. *87*, 6–14. https://doi.org/10.1080/17453674.2016.1235087.
18. Freund, A., Orjalo, A.V., Desprez, P.Y., and Campisi, J. (2010). Inflammatory networks during cellular senescence: causes and consequences. Trends Mol. Med. *16*, 238–246. https://doi.org/10.1016/j.molmed.2010.03.003.
19. Salama, R., Sadaie, M., Hoare, M., and Narita, M. (2014). Cellular senescence and its effector programs. Genes Dev. *28*, 99–114. https://doi.org/10.1101/gad.235184.113.

20. Jeon, O.H., Kim, C., Laberge, R.M., Demaria, M., Rathod, S., Vasserot, A.P., Chung, J.W., Kim, D.H., Poon, Y., David, N., et al. (2017). Local clearance of senescent cells attenuates the development of post-traumatic osteoarthritis and creates a pro-regenerative environment. Nat. Med. *23*, 775–781. https://doi.org/10.1038/nm.4324.
21. Kang, D., Lee, J., Jung, J., Carlson, B.A., Chang, M.J., Chang, C.B., Kang, S.B., Lee, B.C., Gladyshev, V.N., Hatfield, D.L., et al. (2022). Selenophosphate synthetase 1 deficiency exacerbates osteoarthritis by dysregulating redox homeostasis. Nat. Commun. *13*, 779. https://doi.org/10.1038/s41467-022-28385-7.
22. Koike, M., Nojiri, H., Ozawa, Y., Watanabe, K., Muramatsu, Y., Kaneko, H., Morikawa, D., Kobayashi, K., Saita, Y., Sasho, T., et al. (2015). Mechanical overloading causes mitochondrial superoxide and SOD2 imbalance in chondrocytes resulting in cartilage degeneration. Sci. Rep. *5*, 11722. https://doi.org/10.1038/srep11722.
23. Zhao, J., Li, C., Qin, T., Jin, Y., He, R., Sun, Y., Liu, Z., Wu, T., Duan, C., Cao, Y., and Hu, J. (2023). Mechanical overloading-induced miR-325-3p reduction promoted chondrocyte senescence and exacerbated facet joint degeneration. Arthritis Res. Ther. *25*, 54. https://doi.org/10.1186/s13075-023-03037-3.
24. Wang, N., Zhang, X., Rothrauff, B.B., Fritch, M.R., Chang, A., He, Y., Yeung, M., Liu, S., Lipa, K.E., Lei, G., et al. (2022). Novel role of estrogen receptor-α on regulating chondrocyte phenotype and response to mechanical loading. Osteoarthritis Cartilage *30*, 302–314. https://doi.org/10.1016/j.joca.2021.11.002.
25. Worman, H.J., Ostlund, C., and Wang, Y. (2010). Diseases of the nuclear envelope. Cold Spring Harbor Perspect. Biol. *2*, a000760. https://doi.org/10.1101/cshperspect.a000760.
26. Goldman, R.D., Shumaker, D.K., Erdos, M.R., Eriksson, M., Goldman, A.E., Gordon, L.B., Gruenbaum, Y., Khuon, S., Mendez, M., Varga, R., and Collins, F.S. (2004). Accumulation of mutant lamin A causes progressive changes in nuclear architecture in Hutchinson-Gilford progeria syndrome. Proc. Natl. Acad. Sci. USA *101*, 8963–8968. https://doi.org/10.1073/pnas.0402943101.
27. Liu, B., Wang, J., Chan, K.M., Tjia, W.M., Deng, W., Guan, X., Huang, J.D., Li, K.M., Chau, P.Y., Chen, D.J., et al. (2005). Genomic instability in laminopathy-based premature aging. Nat. Med. *11*, 780–785. https://doi.org/10.1038/nm1266.
28. Suo, J., Shao, R., Yang, R., Wang, J., Zhang, Z., Wang, D., Niu, N., Zheng, X., and Zou, W. (2023). Accelerated aging in articular cartilage by ZMPSTE24 deficiency leads to osteoarthritis with impaired metabolic signaling and epigenetic regulation. Cell Death Dis. *14*, 336. https://doi.org/10.1038/s41419-023-05856-3.
29. López-Alonso, I., Blázquez-Prieto, J., Amado-Rodríguez, L., González-López, A., Astudillo, A., Sánchez, M., Huidobro, C., López-Martínez, C., Dos Santos, C.C., and Albaiceta, G.M. (2018). Preventing loss of mechanosensation by the nuclear membranes of alveolar cells reduces lung injury in mice during mechanical ventilation. Sci. Transl. Med. *10*, eaam7598. https://doi.org/10.1126/scitranslmed.aam7598.
30. Li, L., Yang, L., Zhang, K., Zhu, L., Wang, X., and Jiang, Q. (2020). Three-dimensional finite-element analysis of aggravating medial meniscus tears on knee osteoarthritis. J. Orthop. Translat. *20*, 47–55. https://doi.org/10.1016/j.jot.2019.06.007.
31. Das Neves Borges, P., Forte, A.E., Vincent, T.L., Dini, D., and Marenzana, M. (2014). Rapid, automated imaging of mouse articular cartilage by microCT for early detection of osteoarthritis and finite element modelling of joint mechanics. Osteoarthritis Cartilage *22*, 1419–1428. https://doi.org/10.1016/j.joca.2014.07.014.
32. Pan, D., TianYe, L., Peng, Y., JingLi, X., HongZhu, L., HeRan, Z., QingWen, Z., LeiLei, C., ZhenQiu, C., QiuShi, W., and Wei, H. (2020). Effects of proximal fibular osteotomy on stress changes in mild knee osteoarthritis with varus deformity: a finite element analysis. J. Orthop. Surg. Res. *15*, 375. https://doi.org/10.1186/s13018-020-01894-1.
33. Mu, X., Tseng, C., Hambright, W.S., Matre, P., Lin, C.Y., Chanda, P., Chen, W., Gu, J., Ravuri, S., Cui, Y., et al. (2020). Cytoskeleton stiffness regulates cellular senescence and innate immune response in Hutchinson-Gilford Progeria Syndrome. Aging Cell *19*, e13152. https://doi.org/10.1111/acel.13152.
34. Dahl, K.N., Scaffidi, P., Islam, M.F., Yodh, A.G., Wilson, K.L., and Misteli, T. (2006). Distinct structural and mechanical properties of the nuclear lamina in Hutchinson-Gilford progeria syndrome. Proc. Natl. Acad. Sci. USA *103*, 10271–10276. https://doi.org/10.1073/pnas.0601058103.
35. Krishnan, V., Chow, M.Z.Y., Wang, Z., Zhang, L., Liu, B., Liu, X., and Zhou, Z. (2011). Histone H4 lysine 16 hypoacetylation is associated with defective DNA repair and premature senescence in Zmpste24-deficient mice. Proc. Natl. Acad. Sci. USA *108*, 12325–12330. https://doi.org/10.1073/pnas.1102789108.
36. Liu, B., Wang, Z., Zhang, L., Ghosh, S., Zheng, H., and Zhou, Z. (2013). Depleting the methyltransferase Suv39h1 improves DNA repair and extends lifespan in a progeria mouse model. Nat. Commun. *4*, 1868. https://doi.org/10.1038/ncomms2885.
37. Sieprath, T., Corne, T.D.J., Nooteboom, M., Grootaert, C., Rajkovic, A., Buysschaert, B., Robijns, J., Broers, J.L.V., Ramaekers, F.C.S., Koopman, W.J.H., et al. (2015). Sustained accumulation of prelamin A and depletion of lamin A/C both cause oxidative stress and mitochondrial dysfunction but induce different cell fates. Nucleus *6*, 236–246. https://doi.org/10.1080/19491034.2015.1050568.
38. González-Dominguez, A., Montañez, R., Castejón-Vega, B., Nuñez-Vasco, J., Lendines-Cordero, D., Wang, C., Mbalaviele, G., Navarro-Pando, J.M., Alcocer-Gómez, E., and Cordero, M.D. (2021). Inhibition of the NLRP3 inflammasome improves lifespan in animal murine model of Hutchinson-Gilford Progeria. EMBO Mol. Med. *13*, e14012. https://doi.org/10.15252/emmm.202114012.
39. Brayson, D., Frustaci, A., Verardo, R., Chimenti, C., Russo, M.A., Hayward, R., Ahmad, S., Vizcay-Barrena, G., Protti, A., Zammit, P.S., et al. (2019). Prelamin A mediates myocardial inflammation in dilated and HIV-associated cardiomyopathies. JCI Insight *4*, e126315. https://doi.org/10.1172/jci.insight.126315.
40. Gosset, M., Berenbaum, F., Thirion, S., and Jacques, C. (2008). Primary culture and phenotyping of murine chondrocytes. Nat. Protoc. *3*, 1253–1260. https://doi.org/10.1038/nprot.2008.95.
41. Wu, Y., Jin, X., Zhao, X., Wang, Y., Bai, H., Lu, B., Tong, X., Ma, J., and Ma, X. (2022). Computer-aided Design of Distal Femoral Osteotomy for the Valgus Knee and Effect of Correction Angle on Joint Loading by Finite Element Analysis. Orthop. Surg. *14*, 2904–2913. https://doi.org/10.1111/os.13440.
42. Nie, Y., Yu, Q., and Shen, B. (2021). Impact of Tibial Component Coronal Alignment on Knee Joint Biomechanics Following Fixed-bearing Unicompartmental Knee Arthroplasty: A Finite Element Analysis. Orthop. Surg. *13*, 1423–1429. https://doi.org/10.1111/os.12927.
43. Dhaher, Y.Y., Kwon, T.H., and Barry, M. (2010). The effect of connective tissue material uncertainties on knee joint mechanics under isolated loading conditions. J. Biomech. *43*, 3118–3125. https://doi.org/10.1016/j.jbiomech.2010.08.005.
44. Dong, Y., Hu, G., Dong, Y., Hu, Y., and Xu, Q. (2014). The effect of meniscal tears and resultant partial meniscectomies on the knee contact stresses: a finite element analysis. Comput. Methods Biomech. Biomed. Eng. *17*, 1452–1463. https://doi.org/10.1080/10255842.2012.753063.
45. Peña, E., Calvo, B., Martínez, M.A., Palanca, D., and Doblaré, M. (2005). Finite element analysis of the effect of meniscal tears and meniscectomies on human knee biomechanics. Clin. Biomech. *20*, 498–507. https://doi.org/10.1016/j.clinbiomech.2005.01.009.
46. Sathasivam, S., and Walker, P.S. (1997). A computer model with surface friction for the prediction of total knee kinematics. J. Biomech. *30*, 177–184. https://doi.org/10.1016/s0021-9290(96)00114-5.
47. Shah, K.S., Saranathan, A., Koya, B., and Elias, J.J. (2015). Finite element analysis to characterize how varying patellar loading influences pressure applied to cartilage: model evaluation. Comput. Methods Biomech. Biomed. Eng. *18*, 1509–1515. https://doi.org/10.1080/10255842.2014.921814.
48. Sophocleous, A., and Huesa, C. (2019). Osteoarthritis Mouse Model of Destabilization of the Medial Meniscus. Methods Mol. Biol. *1914*, 281–293. https://doi.org/10.1007/978-1-4939-8997-3_15.
49. Krenn, V., Morawietz, L., Burmester, G.R., Kinne, R.W., Mueller-Ladner, U., Muller, B., and Haupl, T. (2006). Synovitis score: discrimination between chronic low-grade and high-grade synovitis. Histopathology *49*, 358–364. https://doi.org/10.1111/j.1365-2559.2006.02508.x.

STAR★METHODS

KEY RESOURCES TABLE

REAGENT or RESOURCE	SOURCE	IDENTIFIER
Antibodies		
ZMPSTE24 polyclonal antibody	NOVUS	(Novus Cat# NB100-2387, RRID:AB_10003134)
p21 polyclonal antibody	Proteintech	(Proteintech Cat# 10355-1-AP, RRID:AB_2077682)
Col2a1 polyclonal antibody	Abcam	(Abcam Cat# ab34712, RRID:AB_731688)
Lamin A/C monoclonal antibody	Cell Signaling Technology	(Cell Signaling Technology Cat# 4777, RRID:AB_10545756)
Mmp13 polyclonal antibody	Abcam	(Abcam Cat# ab39012, RRID:AB_776416)
Sox9 polyclonal antibody	Abcam	(Abcam Cat# ab185966, RRID:AB_2728660)
p16 monoclonal antibody	Abcam	(Abcam Cat# ab211542, RRID:AB_2891084)
GAPDH monoclonal antibody	Cell Signaling Technology	(Cell Signaling Technology Cat# 5174, RRID:AB_10622025)
Chemicals, peptides, and recombinant proteins		
SF488-labeled phalloidin	Solarbio	CA1640
Goat Serum	Solarbio	SL038
DMEM/F12 medium	Gibco	11320033
Fetal bovine serum	Gibco	10099141C
SA-β-gal staining kit	Beyotime	C0602
RNA extraction kit	Omega	R6812-01
DHE probe	Med Chem Express	HY-D0079
Experimental models: Cell lines		
ATDC5	Cell Bank of the Chinese Academy of Sciences	(RCB Cat# RCB0565, RRID:CVCL_3894)
Software and algorithms		
ImageJ Version 1.53 for Mac	National Institutes of Health	https://www.nih.gov/
GraphPad Prism Version 8 for Mac	GraphPad Software	https://www.graphpad.com/

RESOURCE AVAILABILITY

Lead contact

Further information and requests for resources and reagents should be directed to and will be fulfilled by the lead contact, Zanjing Zhai (zanjing_zhai@163.com).

Materials availability

Zmpste24 overexpression ATDC5 cells can be obtained from the lead contact upon request.

Data and code availability

Experimental data reported in this manuscript will be shared by the lead contact upon request.

This paper does not report original code.

Any additional information required to reanalyze the data reported in this paper is available from the lead contact upon request.

EXPERIMENTAL MODEL AND STUDY PARTICIPANT DETAILS

Human cartilage specimen collection and preparation

The ethics committee of our hospital approved all the studies involving human articular cartilage (SH9H-2019-T190-1). All patients were from Chinese Han population.

Human tibial plateaus were collected from varus patients undergoing TKA (Total knee arthroplasty) and demographic statistics of all patients aere detailed in Table 3. The tibial plateau was divided into four areas: the anteromedial (AM), anterolateral (AL), posteromedial (PM), and posterolateral (PL). In the center of each area, we drilled an osteochondral plug with an area of 0.5 cm * 0.5 cm. The removed plugs were fixed in 4% paraformaldehyde for further analysis.

Animals and surgical procedures

C57BL/6J mice were obtained from the Shanghai Ninth People's Hospital Animal Center, and the animal experimental procedures were approved by the Ethics Committee of Shanghai Ninth People's Hospital (SH9H-2023-A799-1). Twelve 12-week-old male C57BL/6J mice were randomly divided into two groups: sham and destabilization of the medial meniscus (DMM). The mice that underwent DMM surgery were anesthetized with isoflurane. Microscissors were used to cut the medial meniscotibial ligament to destabilize the medial meniscus. The mice were sacrificed 12 weeks after surgery and the right knee joint was collected and fixed in 4% paraformaldehyde for subsequent analysis.

Cell culture and reagents

Murine chondrocytes were extracted from newborn C57BL/6J mice following the protocol described by Gosset et al.[40] Chondrocytes were cultured in Dulbecco's modified eagle medium (DMEM)/Ham 's F12 with 4.5 g glucose/L, 10% fetal bovine serum (FBS), and 1% penicillin–streptomycin (Gibco, Thermo Fisher Scientific, United States).

Overexpression of Zmpste24 in ATDC5 cells

The mouse chondrocyte cell line ATDC5 was purchased from the Cell Bank of the Chinese Academy of Sciences (Shanghai, China) and cultured in DMEM with 4.5 g glucose/L, 5% fetal bovine serum (FBS), and 1% penicillin–streptomycin. Zmpste24 overexpression lentivirus was provided by OBIO, Shanghai, and an optimal multiplicity of infection (MOI) of 20 was used to infect the cells. Puromycin was added 48 h after infection to screen for a stable Zmpste24 overexpression cell line.

METHODS DETAILS

Imaging data acquisition and geometric modeling

All imaging data were approved by the ethics committee of Shanghai Ninth People's Hospital (SH9H-2019-T190-1). A patient with OA and knee varus underwent Computed Tomography (CT) and Magnetic Resonance Imaging (MRI) of the right knee. An X-ray image of a representative patient with varus knees is shown in Figure 1A. Data were imported into the Mimics software (Version 18.0), and the geometry of the bone was remodeled. Soft tissue reconstruction was performed using MRI data3-matic medical (version 9.0, Belgium) to refine and assemble the geometric models (Figure 1B). Considering the Saint-Venant principle, the area of interest in the lower limbs was considered the research object, as per the study by Wu et al.[41] (Figure 1C).

FEA and material models

STL data were converted into the IGES format using Geomagic Wrap (Version 2017, North Carolina, USA) and imported into HyperMesh (Version 14.0, Altair, USA), where assembly and meshing were completed. Three-node 3D rigid triangular facet elements (R3D3) were used for bony tissues, whereas for other soft tissues a 10-node quadratic tetrahedron (C3D10HM) element was used to improve computational efficiency. Referring to Nie's study[42] on mesh convergence analysis, the mesh size of bones was taken as 2.0 mm, and that of cartilage and ligaments was taken as 0.5-1.0 mm. The three-dimensional mesh model is shown in Figure 1D. The elastic modulus of the linear elastic model of the cartilage was 15 Mpa, and Poisson's ratio was 0.475.[43] The meniscus was modeled as a transversely anisotropic material, and the material parameters are listed in Table 1.[44] The ligaments were assumed to be isotropic and hyperelastic, represented by an incompressible neo-Hookean behavior[43,45] and the strain energy function is

$$\Psi = C1(\bar{I}_1 - 3)$$

C1 is the bulk material constant related to the shear modulus μ ($C1 = 2/\mu$). where $\bar{I}_1$ is the first modified invariant of the right Cauchy-Green strain tensor. The material constants are listed in Table 2.

Loads, boundary conditions, and contact interrelationships

The knee joint was simulated in a standing posture with the femoral condyle set as the reference point for the femoral rigid body. Subsequently, a vertical downward load of 1150 N was applied at this point, as shown in Figure 1E. This load corresponds to the load when the lower limb is fully extended during a gait cycle,[44,46] with the tibia and fibula limiting all degrees of freedom and the femur and other soft tissues being free.

Friction contact was adopted between the cartilages with a friction coefficient of 0.02.[47] Binding constraints were also applied to other tissues.

Micro-CT scanning

After fixation for 48 h, right knee joints were scanned with a micro-CT scanner (Skyscan 1072, Belgium) at a resolution of 10.5 μm, with a 55 kVp source and 145 μ Amp current. Micro-CT data were analyzed using CT-An (Bruker, Germany) by a researcher who was blind to group allocation and representative subchondral bone sections were remodeled using CT-Vox software (Bruker, Germany).

Histology, immunohistochemistry (IHC), and immunofluorescence (IF) staining

Serial sections of 5 μm thickness in a sagittal plane were obtained and cartilage was stained with safranine O/fast green and toluidine blue to evaluate cartilage clefts. The OARSI score was evaluated according to the Sophocleous standards.[48] Hematoxylin and eosin staining was used to evaluate synovial inflammation, and the synovitis score was calculated using Krenn's principle.[49]

For IHC and IF staining, sections were incubated with primary antibody Anti-p21 (10355-1-AP, Proteintech), anti-Col2a1 (ab34712, Abcam) and anti-Zmpste24 (NB100-2387, Novus) overnight at 4°C. For IHC staining, the sections were stained with horseradish peroxidase-conjugated secondary antibodies. For IF staining, the sections were incubated with Alexa Fluor 555 or 488 conjugate secondary antibody. Images were acquired using the DM4000B microscope (Carl Zeiss).

For F-actin staining, the chondrocytes were incubated with SF488-labeled phalloidin for 30 min. For cell immunofluorescence, after fixation, permeabilization, and blocking with 10% goat serum, cells were incubated with primary antibody for Zmpste24 (NB100-2387, Novus) or Lamin A/C (4777, CST) overnight at 4°C. The cells were then incubated with Alexa Fluor 555 or 488 conjugate secondary antibody (Abcam) for 1 h. Fluorescent images were captured using a DM4000B microscope (Zeiss, Oberkochen, Germany).

Cyclic tensile strain loading of chondrocytes

A commercially available cell stretch system, CellTank (Hangzhou Biaomianli Technology Co LTD, China) was used to exert different magnitudes of cyclic tensile strain on chondrocytes (0.5 Hz; 0, 5, and 20%). Chondrocytes were seeded at a density of 4×10^6 cells/chamber in soft-stretch chambers coated with fibronectin. They were stretched for 12 h or 24 h in a CO_2 incubator after attaching to the chamber. The running state details of CellTank are provided in the Supplementary Materials.

Senescence-associated-β-galactosidase (SA-β-gal) staining

Cellular senescence was evaluated using SA-β-gal staining. Chondrocytes were treated with different concentrations of CTS (0, 5, or 20%) for 24 h before staining. After fixation with 4% paraformaldehyde for 10 min, stretched cells were stained with a SA-β-gal staining kit (Beyotime, China). Images were taken using a Zeiss microscope.

Detection of reactive oxygen species (ROS)

After treated with 20% CTS for 24h, chondrocytes were incubated with 5 μM DHE probe (HY-D0079; Med Chem Express, China) for 30 min at 37°C. After rinsing with warm PBS for three times, fluorescent images were captured using a DM4000B microscope (Zeiss, Oberkochen, Germany). ImageJ was used for semi-quantitative analysis of ROS intensity.

Protein extraction and western blot analysis

After treatment with different strains (0%, 5%, and 20%) for 24 h, the cells were lysed with RIPA buffer. For western blot analysis, 20 μg protein per well was loaded onto SDS-PAGE gels and then transferred to a polyvinylidene fluoride (PVDF) membrane (Millipore, Germany). The membranes were incubated overnight with the corresponding primary antibodies. After incubation with secondary antibodies for 2 h, the membranes were visualized using an Odyssey V3.0 image scanner (Li-COR. Inc. USA). Quantitative Real-time PCR (qRT-PCR)

For qRT-PCR, a total RNA kit (R6812-01HP, Omega Bio-tek Inc., Norcross, GA, United State) was used to extract total RNA from the treated cells. Subsequently, 1000 ng of cDNA was prepared according to the cDNA synthesis kit protocol (Takara, Japan). A total 10 μL mix, composed of 3.6 μL ddH2O, 1 μL diluted cDNA, 0.2 μL upstream primer, 0.2 μL downstream primer, and 5 μL SYBR premix (Selleck, USA), was added to each well of a 384-well plate. RT-qPCR was performed using an ABI 7500 Sequencing Detection System (Applied Biosystems, Foster City, CA, USA). All primer sequences used for the target genes are listed in Table S1.

QUANTIFICATION AND STATISTICAL ANALYSIS

Statistical analysis

All statistical analyses were performed using SPSS version 19.0 (SPSS Inc., Chicago, IL.). For data with a normal distribution, the unpaired Student's t-test was used to compare the two groups. Comparisons between three or more groups were performed using one-way ANOVAs and Student-Newman-Keuls post hoc tests. For non-normally distributed data, the Mann-Whitney and Kruskal-Wallis tests were used to compare two groups or multiple groups. Pearson's correlation analysis was used to test the correlation between two continuous variables and obtain regression equations using simple linear regression methods. All the statistical charts were designed and drawn using GraphPad Prism 8 (GraphPad Software Inc., San Diego, CA, USA). Statistical significance was set at $P < 0.05$.